

**Silicon Crystal Surface Temperature:  
Computational and Radiometric Studies**

Ali M. Khounsary, Tuncer M. Kuzay, and George A. Forster  
Argonne National Laboratory, Argonne, IL 60439

SUMMARY

The surface temperature of the three-channel, gallium-cooled Cornell silicon crystal is evaluated for the given system configuration and specifications. The THTB thermal-hydraulic program is used for the numerical solution of the problem, and the results are to be compared with the radiometric measurements obtained at Cornell.

The Inframetrics IR camera model 525 used in the Cornell experiments is critically tested at Argonne and the necessary correlation curves (relating camera readings to actual temperature of an isothermal silicon crystal) are obtained. In addition, the blackbody correlation curves provided by Inframetrics Corp. are reproduced and verified.

The suitability and reliability of IR radiometry in the case of partially transparent bodies (such as silicon in the IR region of the spectrum) are discussed and procedures for data collection and interpretation are recommended. It is indicated that to infer the crystal surface temperature accurately, a number of factors (mostly related to the partial transparency of the crystal) must be taken into account. These are outlined in some detail. Theoretical developments are deferred, since they are complicated and since we still favor the coating method as the simplest and most reliable solution approach.

## 1.0 INTRODUCTION

In the March 11, 1988, meeting of the APS Study Group on High Heat Loads in X-Ray Optics, a priority task identified was the modeling and analysis of the heat transfer aspects of the CORNELL three-channel and the ANL five-channel silicon crystals. These crystals are cooled by water or gallium. In addition, the IR data obtained in the CHESS experiments at Cornell were to be examined and verified. System specifications and input parameters were discussed and finalized during the meeting.

Our initial modeling of the CHESS crystal yielded temperatures on the surface of the crystal far in excess of those indicated by the Cornell IR measurements as presented at the meeting (Fig. 1). In fact, the computed maximum temperature difference on the surface of the CHESS crystal was found to be as much as three times the values presented at that meeting. We thoroughly checked our modeling, input data, and the computations. Nothing that could explain this discrepancy was found.

We then began to investigate the reliability of the supplied IR measurements. One of the authors, G. Forster, noted the transparency of the silicon crystal to IR radiation. Then, we surmised that the experimental technique and the data obtained might be suspect. Our suspicion was further reinforced when we reviewed the literature on the radiative properties of silicon crystals in the infrared region of the spectrum (see Figures 2 and 3). The steep variations in these properties, particularly in the infrared region, and the corrections needed to account for the transmittance and reflectance of silicon seem to preclude unaided and direct thermometric measurement of the silicon crystal. Another author, A. Khounsary, suggested that the silicon crystal be coated with a layer of a material opaque to infrared.

The IR scanner (Inframetrics model 525) used at Cornell is an "8-12" unit. This means that it is most sensitive to and suitable for (blackbody) temperature measurements in the 20-100°C range. Unfortunately, it is in this very range that a silicon crystal exhibits steep variations in its radiative properties. Therefore, if the crystal is not coated, the raw data taken by the infrared scanner must be processed and interpreted to infer the actual temperatures, a laborious (and unnecessary) task in view of the strong frequency dependence of the radiative properties of silicon crystals in the spectral range of interest. On the basis of these considerations, it was then decided to run some temperature measurement tests at the ANL/Bldg. 223 laboratory. Experimental apparatus consisting of a piece of spare silicon crystal with a Peltier-effect back was set up. A thermocouple was also contact-mounted on the frontal surface of the crystal to independently measure the surface temperature at that location.

Inframetrics, Inc., was contacted to seek advice on possible opaque coatings. They suggested black vinyl electrician's tape, spray foot powder, and dye penetrant developer powder; in addition, we also considered carbon black and candle soot as acceptable candidates. These materials are all opaque to infrared radiation, have emissivities in excess of 0.9 and are readily available. The black electrician's tape and the dye penetrant developer powder (in patches) were used in our experiment. Both were equally practical, but the tape would lose its adhesiveness and peel off at higher operating temperatures. The thermocouple itself was also coated so that its temperature would also be monitored to assure proper surface contact, and thus accurate reading of the surface temperature.

Our preliminary experimental data indicated a linear correlation between the IR scanner readings and the thermocouple measurements.

As a result of these experiments, therefore, we believe that the source of the three-fold difference between our thermal-hydraulic modeling results and the Cornell IR temperature measurements are due to erroneous interpretation of IR readings. The actual temperature rise along the surface of the three-channel crystal is about three times the values presented at the March 11 meeting. Thus, the correct value is in the 40-45°C range (assuming that the flow rate, channel and footprint dimensions, power level, etc. that are provided are accurate).

Follow-up IR calibration studies in the laboratory and accompanying analytical work verified the above conclusions. This follow-up work is detailed below.

## 2.0 SYSTEM SPECIFICATIONS AND INPUT DATA

The dimensions of the crystal under study and other systems specifications are included in Fig. 4. The incident beam in this particular case makes a 14.3-degree angle with the top of the crystal. In a plane perpendicular to the direction of incidence and at the center of the beam, orthogonal coordinates  $x'$  and  $y'$  are chosen. The incident beam has a spatial power distribution which is Gaussian along  $y'$ -direction and parabolic along  $x'$ -direction. The power contained in an elemental area  $dx'dy'$  is given by

$$P(x', y') dx' dy' = A \left[ \left[ 1 - (1-a) \frac{x'^2}{x_o^2} \right] dx' \right] \left[ \frac{1}{\sigma\sqrt{2\pi}} e^{-\frac{y'^2}{2\sigma^2}} dy' \right] \quad (1)$$

where

$dy'$  =  $\sin\theta$   $dy$  (note the coordinate system  $xyz$  in Figure 4)

$\theta$  = the angle between the direction of incidence and  $y$ -axis

$a$  = cut-off height of the beam's parabolic profile

(here,  $a = 0.3$ ; see Fig. 5)

$A$  = constant of proportionality (to be determined)

$2x'_0$  = beam footprint width along  $x'$ -axis

$\sigma$  = standard deviation of the beam's Gaussian profile (to be determined)

The unknown quantities  $A$  and  $\sigma$  are chosen such that

(1) total incident power =  $\frac{375}{2} = 187.5$  W,

(2) 50% of the source power is contained within  $y' = (-1,1)$  mm band around the Gaussian peak in the beam, and

(3) the beam's cross-section has dimensions  $2x'_0$  and  $2y'_0$  ( $x'_0 = 14$  mm  $\equiv 0.5512$  in and  $y'_0 = 1.5$  mm  $\equiv 0.0591$  in).

Thus, the spatial distribution of the incident beam in a plane perpendicular to the directions of incidence can be written as

$$P(x', y') = P_0 \left[ 1 - (1-a) \frac{x'^2}{x_0'^2} \right] e^{-\frac{y'^2}{2\sigma^2}} \quad (2)$$

where

$$P_0 = \text{peak power} = 6.84 \text{ W/mm}^2 \equiv 4413 \text{ W/in}^2$$

$$\sigma = 1.48 \text{ mm} \equiv 0.0583 \text{ in}$$

Note that since  $y_0' = 1.5$  mm and  $\sigma = 1.48$  mm, almost all the energy is concentrated within one standard deviation around the Gaussian peak.

The power distribution is integrated over appropriate limits (in the  $x'-y'$  plane) to evaluate the incident power on various footprint nodes.

## 2.1 Nodal Distribution

The initially assumed nodal distribution in the crystal is shown in Fig. 6. The temperature distribution on the top surface of the crystal when the incident power is uniform is shown in Fig. 7. A maximum temperature of 97.2°C is obtained. The gallium inlet temperature is 50°C.

The requirement for a more accurate temperature evaluation of the upper layers of the crystal is satisfied by considering a thermally equivalent system shown in Fig. 8. This simulation allows finer nodes and yields a more accurate surface temperature distribution. The incident Gaussian-parabolic power distribution (Eq. 2) is resolved into 12 divisions along its parabolic profile and 5 divisions along its Gaussian profile (Fig. 8).

The THTB results for the top surface temperature of this configuration (Fig. 8) are displayed in Fig. 9. A maximum temperature of 107.4°C on the surface close to the center is obtained. The gallium inlet temperature is again 50°C. The temperature variation on the surface of the crystal ranges from a high of 107.4 to a low of 50.1°C. The incident beam's footprint is also shown in Fig. 9. It must be noted that as a result of the non-uniform incident power distribution and the finer nodes taken on the crystal surface, more accurate and (in this particular case) higher surface temperatures are obtained.

The temperature distribution obtained is accurate to within several degrees. The limitation on accuracy is mainly a consequence of the

restriction on the number of available nodes and the simulation discussed above. The overall dependence of the surface temperature on various system parameters is along the lines discussed in our March memorandum [Kuzay and Khounsary, 1988]. In particular, our computations show that a reduction of gallium inlet temperature from 50°C to 30°C would affect the overall temperature differentials in the system by only a couple of degrees.

### 3.0 INFRARED PYROMETRY

The Inframetrics system model 525 used in the APS experiments responds to photons in the 3-13  $\mu\text{m}$  band, but it is particularly sensitive to those in the 8-12 $\mu\text{m}$  range. The system output, in the form of line-scans or isotherms displayed on the video terminal, is related to the temperature of the viewing object via the object's emissivity and through (almost linear) empirical correlation curves supplied by Inframetrics. These curves are reproducible and should be checked to ensure proper experimental setup and procedures. The model 525 system can discriminate (on the video display) temperature differences of as little as 0.5°C across the field of view (for black bodies). Absolute temperatures can be measured with the same accuracy if a suitable reference source is available.

For an opaque body, such measurements are simple, provided the emissivity of the body is known. Complications, however, arise in the IR temperature measurement of partially transparent bodies (PTB's). In such cases the following points must be taken into account:

- (1) The photons intercepted by the detector are no longer the ones emitted on the surface of the object. They come from throughout the medium and also from the background (Fig. 10). In addition, if the medium is

nonisothermal (as in the present case) the non-uniform distribution of internal emission must be taken into account.

- (2) The silicon crystal under discussion here is neither isothermal nor opaque, and therefore an emissivity in the usual sense cannot be defined. However, we can define a radiometric emittance which measures the ratio of the radiance of the sample to that of a blackbody at the same temperature and under the same geometric and viewing conditions.
- (3) Silicon has a high ( $\sim 3.5$ ) index of refraction (see Fig. 11). This means that in addition to emission and transmission, reflection and refraction must also be taken into account. It is also noted that the emission rate in silicon is  $n^2$  times that of a blackbody at the same temperature,  $n$  being the index of refraction.

The theoretical development of a model for the determination of radiative intensity exiting the surface of the silicon crystal is rather involved, especially since other factors, such as temperature dependence of the radiative properties, conduction and convection in the crystal, non-uniform incident radiation beam, etc., are also involved. Therefore, it is advantageous to attempt an experimental solution of this problem. This is briefly discussed below.

#### 4.0 RADIOMETRIC CALIBRATION

Understanding the various factors involved in the transfer of radiation in silicon crystals as described above is important in the development of an appropriate experimental setup for system calibration. With these factors in mind, the following set of experiments were conducted to relate the surface temperature of an isothermal crystal to camera readings.

#### 4.1 Correlation Curves for the Silicon Crystal: Experiments and Results

Experiments were conducted at ANL, Bldg. 223, to obtain correlation curves relating the surface temperatures to camera system measurements. A five-channel silicon crystal was used. Water from a constant temperature bath was passed through the crystal channels to maintain a constant temperature in the crystal for each round of measurements. A "blackbody" was also introduced in series in this closed loop as a reference source (Fig. 12).

In the first experiment, the system IR response to the "blackbody" in the flow loop at various temperatures was recorded. These measurements are plotted against the true temperature of the blackbody (Fig. 13, Data I). An almost linear relationship (with a slope of  $\frac{1}{5.5}$ ) matching the calibration curves provided in the Inframetrics manual is obtained. Therefore, the surface temperature differentials of a blackbody can be obtained by multiplying the camera readings (on the 50 scale) by a factor of 5.5. For an absolute temperature measurement, a reference source is needed.

In the next experiment, the silicon crystal was partially coated on the front and back surfaces (Fig. 14). Readings from the three sections of the crystal and also the blackbody in the flow loop were taken at various isothermal-bath temperatures. These are also plotted in Figure 13. Note that the blackbody measurements (data II) are again on the same line drawn through data I. Since the blackbody source and the silicon crystal are at the same temperature, it follows from the front-coated section measurements (Fig. 13) that the coated segment of the crystal behaves effectively as a blackbody surface. Also note that front coating yields the true surface temperature, whether or not the crystal is isothermal.

The radiometric measurements from the uncoated part of the crystal show apparent temperatures less than that of the blackbody source. However, as

seen in Fig. 13, there still exists an almost linear correlation between radiometric readings and the actual surface temperatures. The slope of this line in this particular case is  $\frac{1}{8.1}$ . Therefore, temperature differentials on the surface can be estimated by multiplying the camera readings by a factor of 8.1; otherwise, they are underestimated by this factor. It is very important to realize, however, that this correlation curve can be used to obtain the surface temperature of a silicon crystal only if the crystal is isothermal and has the same configuration as the one used in this experiment. Otherwise, appropriate correlation curves must first be obtained.

## 5.0 CONCLUSIONS

The infrared camera used for surface temperature measurements at Cornell can provide accurate results provided the required correlation curves as discussed are obtained. Our numerical solution of the problem, presented in this memorandum, is accurate to within several percentage points and can be compared with the radiometric results once the latter become available.

It is important to recognize that radiometric correlation curves for uncoated crystals in general depend on the experimental setup, background radiation, thickness of the layer, temperature distribution within the crystal along the line-of-sight of the camera, etc. Thus, if coating must be avoided, we should obtain correlation curves for any crystal specimen of interest under conditions as close as possible to those prevailing in the actual experimental setup. It is only then that the radiometric measurements can be correctly interpreted. We also think that to establish the accuracy of such correlations, it may be necessary to obtain a parallel analytical solution to the problem as well.

References

Jamieson, J. A., et al., Infrared Physics and Engineering, McGraw-Hill, New York, 1963.

Kuzay, T. M., and A. M. Khounsary, "Cornell-CHESS Undulator Analysis," ANL Memo, March 22, 1988.

Quinn, T. J., Temperature, Academic Press, New York, 1983.

Svet, D. Y., Thermal Radiation: Metals, Semi-Conductors, Ceramics, Partially Transparent Bodies, and Films, Consultants Bureau, New York, 1965.

Smither, R. K., Private communication, 1988.

Touloukian, Y.S., (ed.), Thermophysical Properties of Matter, IFI/PLENUM, New York, 1970.

Wolfe, W.L., and G. J. Zissis (ed.), The Infrared Handbook, Office of Naval Research, Department of the Navy, Washington, D.C., 1978.

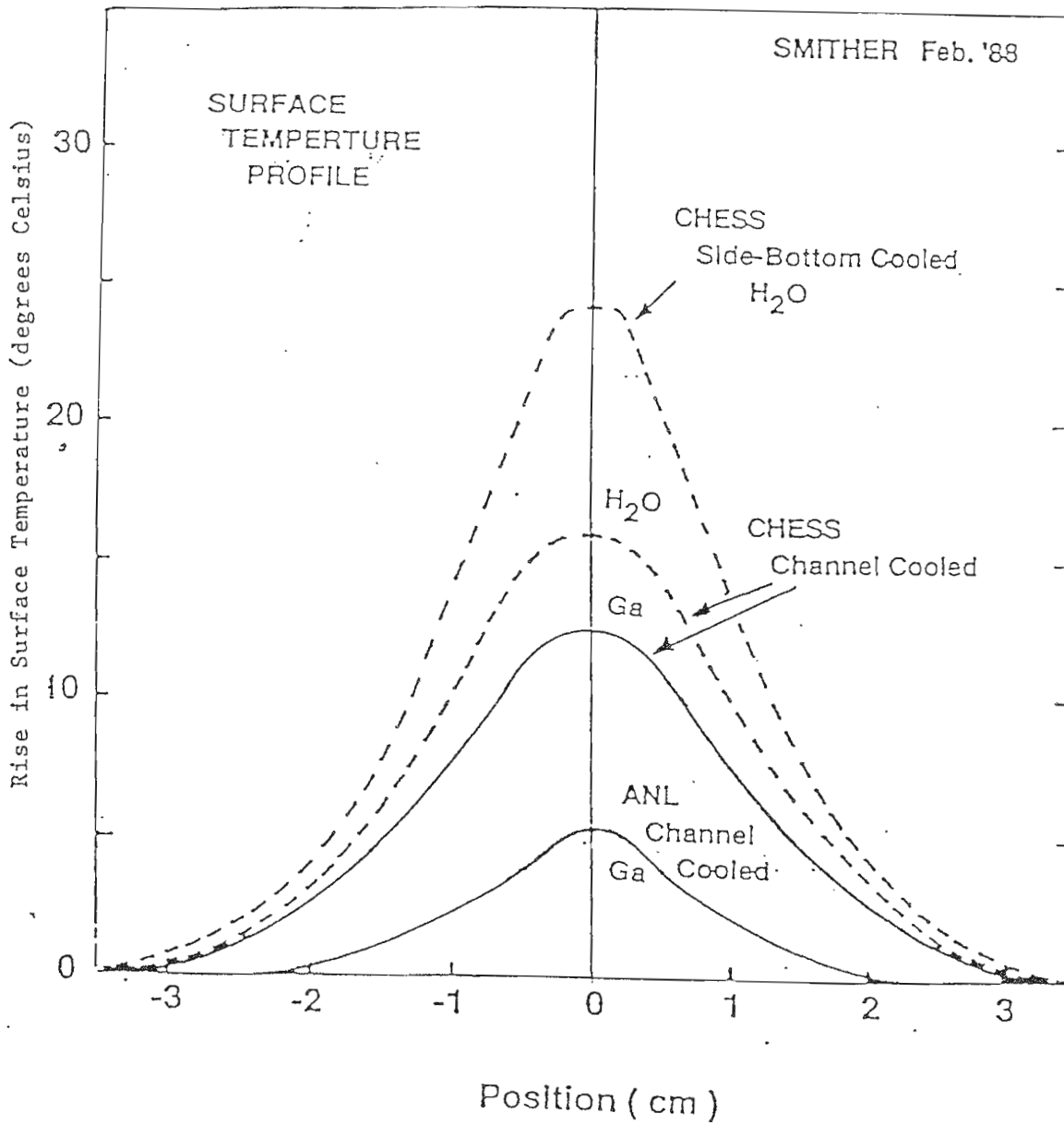


Fig. 1. Silicon Crystal Surface Temperature Profile Data (borrowed from Smither, 1988)

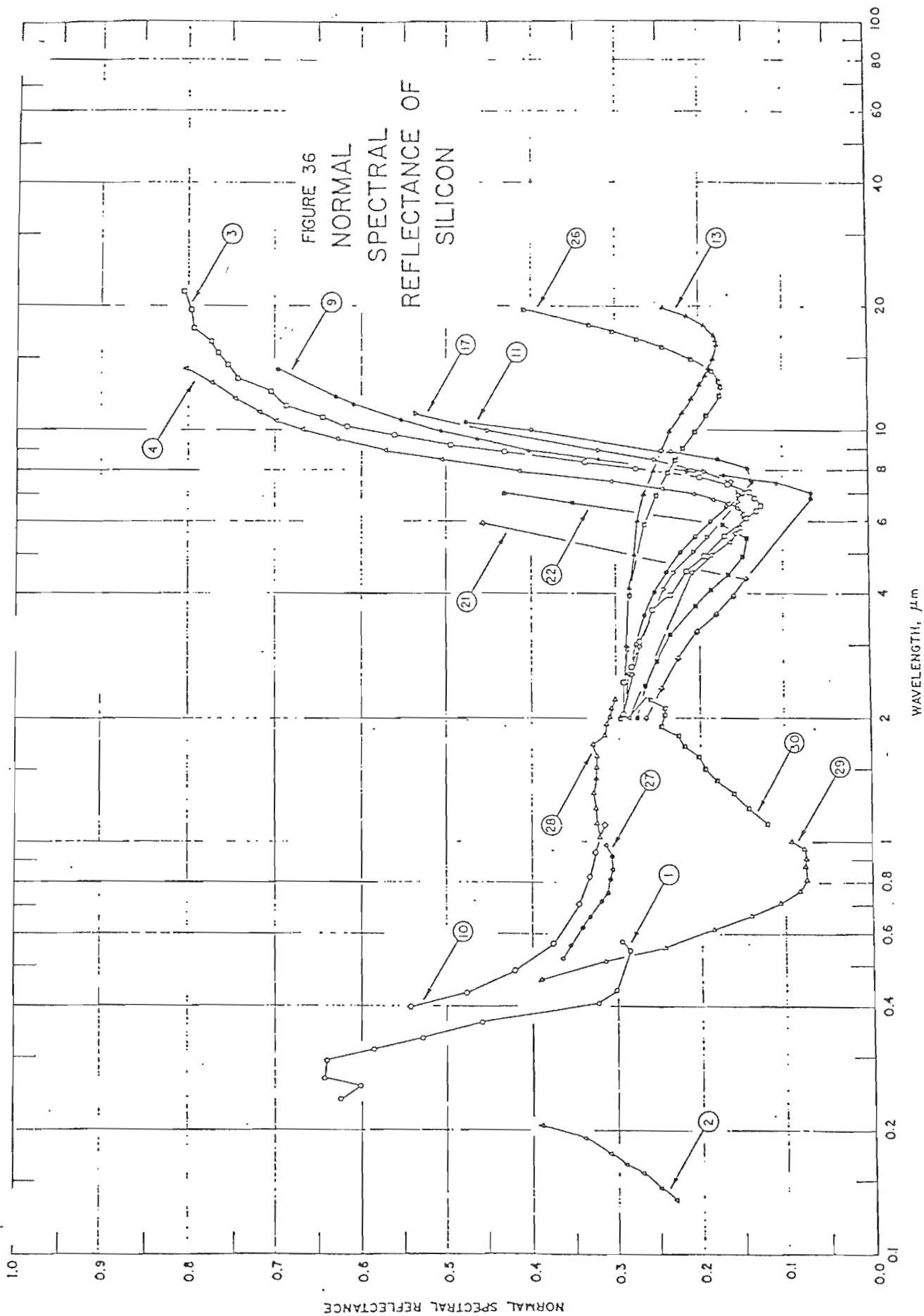


Fig. 2. Normal Spectra Reflectance of Silicon (Touloukian, Properties of Matter)

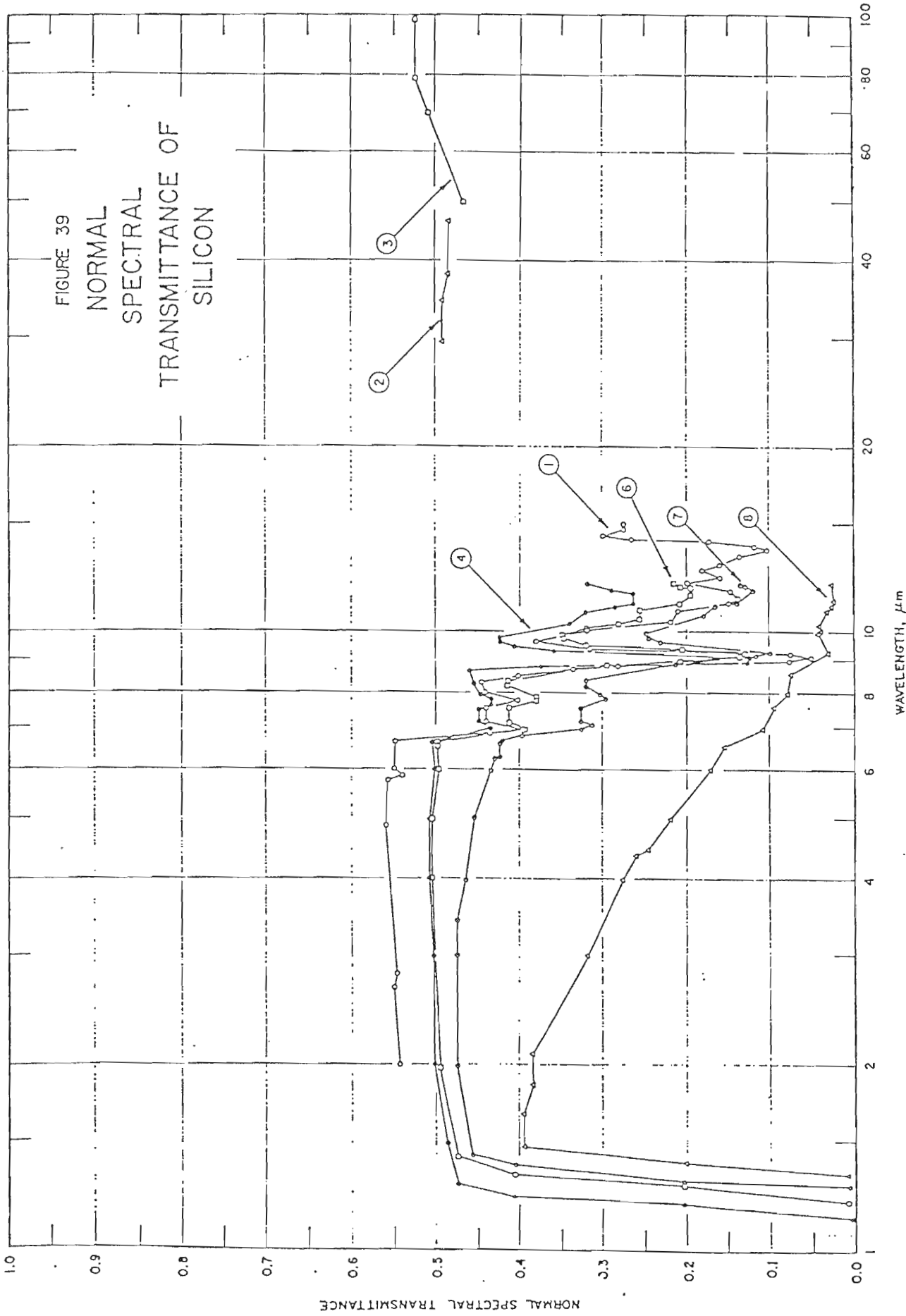


Fig. 3. Normal Spectral Transmittance of Silicon (Touloukian, 1970)

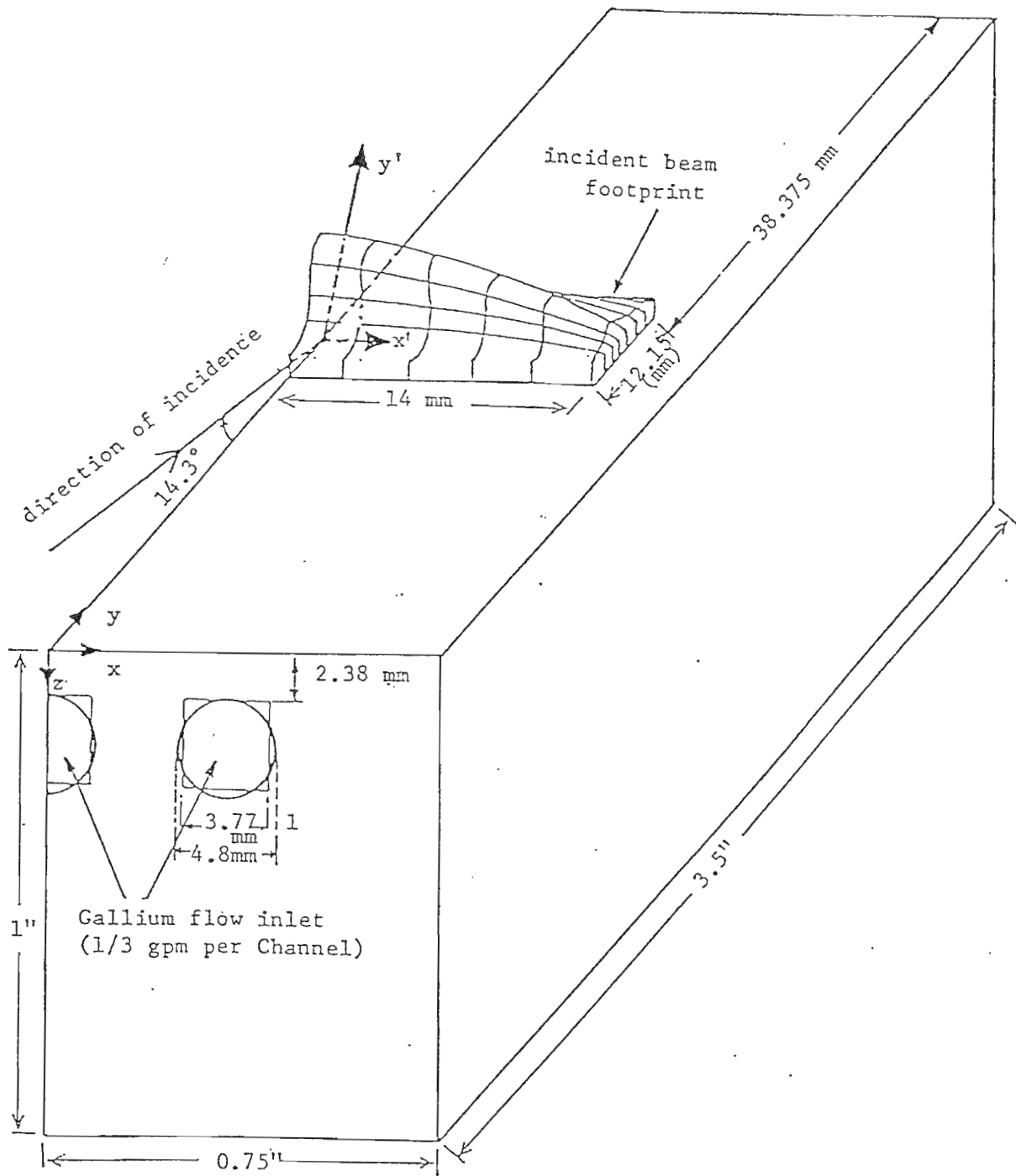
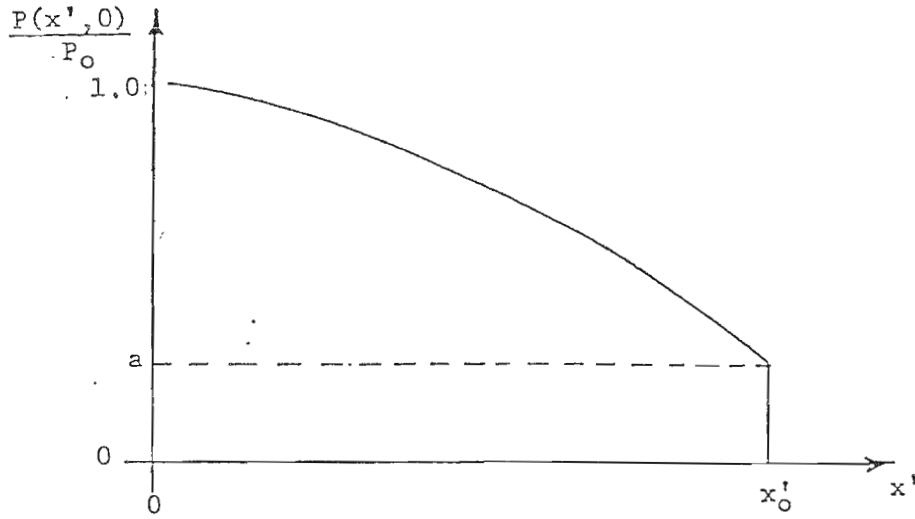
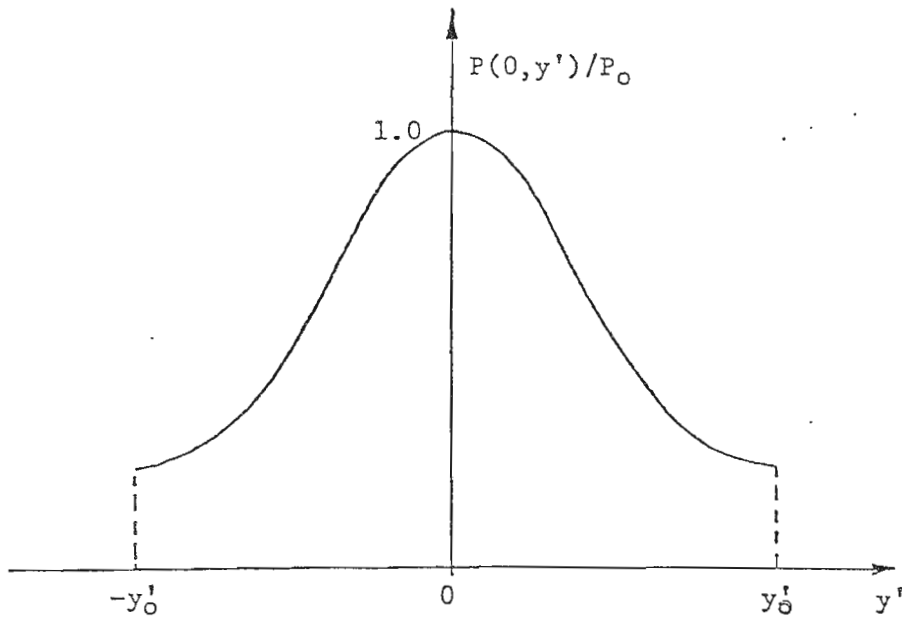


Fig. 4. A sketch of the right half of the silicon crystal. The spatial power distribution of the incident beam (on the footprint) is also shown.



(a)



(b)

Fig. 5. The spatial parabolic (a) and Gaussian (b) profiles of the incident beam along the  $x'$  and  $y'$ -axes, respectively.

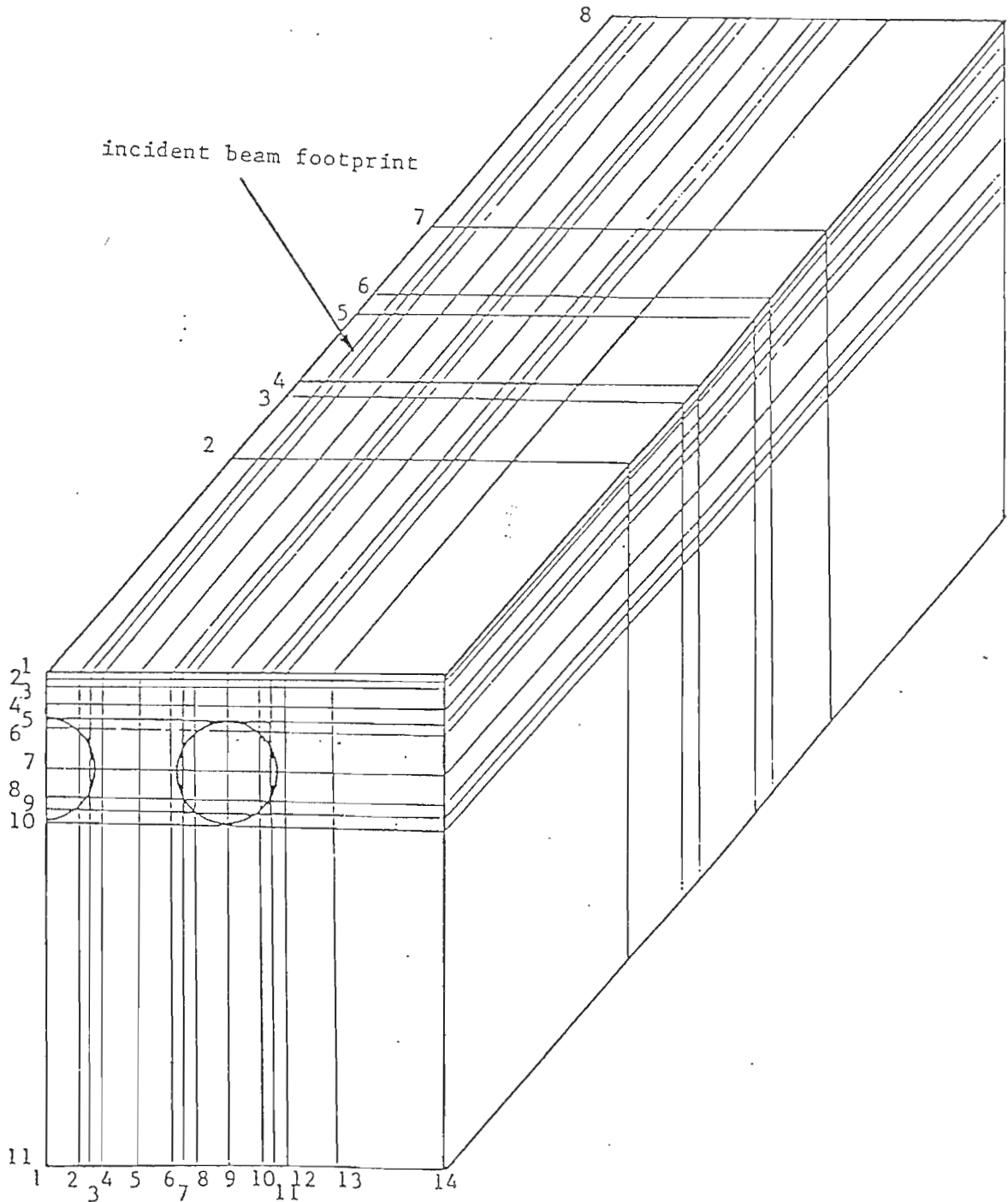


Fig. 6. Initial nodal distribution in the 3-channel silicon crystal.

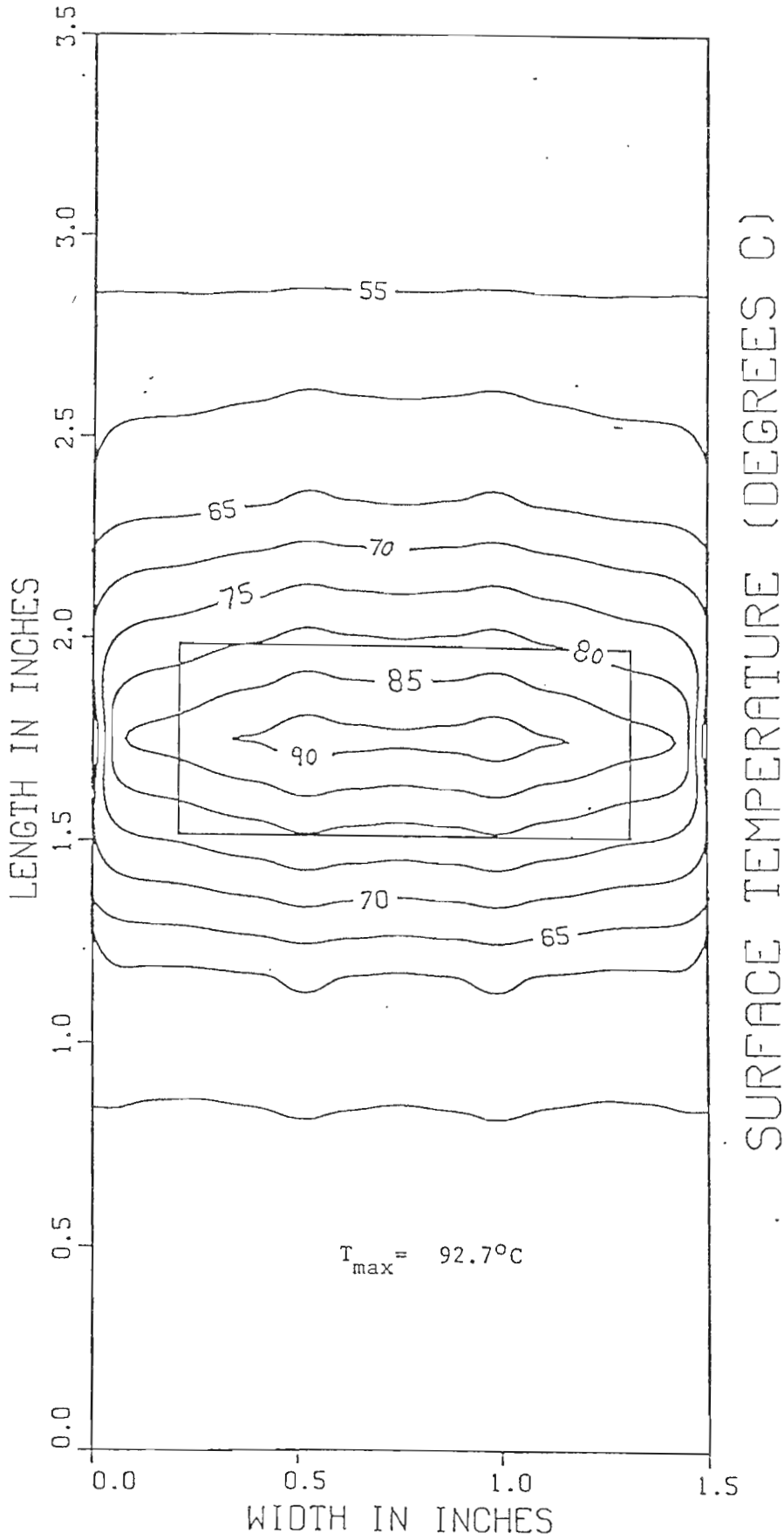


Fig. 7. The temperature distribution on the surface of the silicon crystal shown in Fig. 3. A uniform incident power distribution is assumed. The beam footprint is also shown.

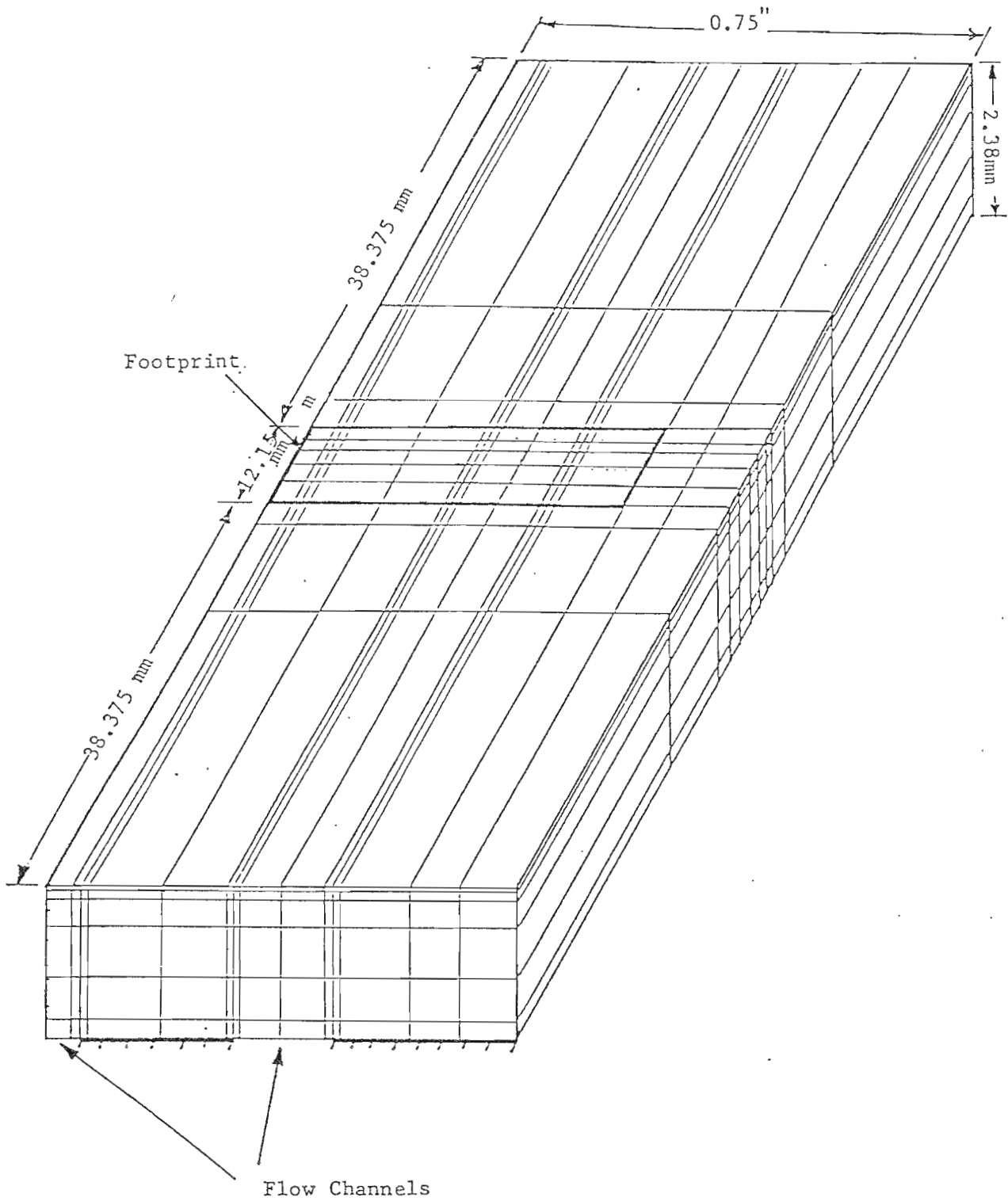


Fig. 8. A simulated configuration with finer nodal distribution for the silicon crystal.

## SURFACE TEMPERATURE (DEGREES C)

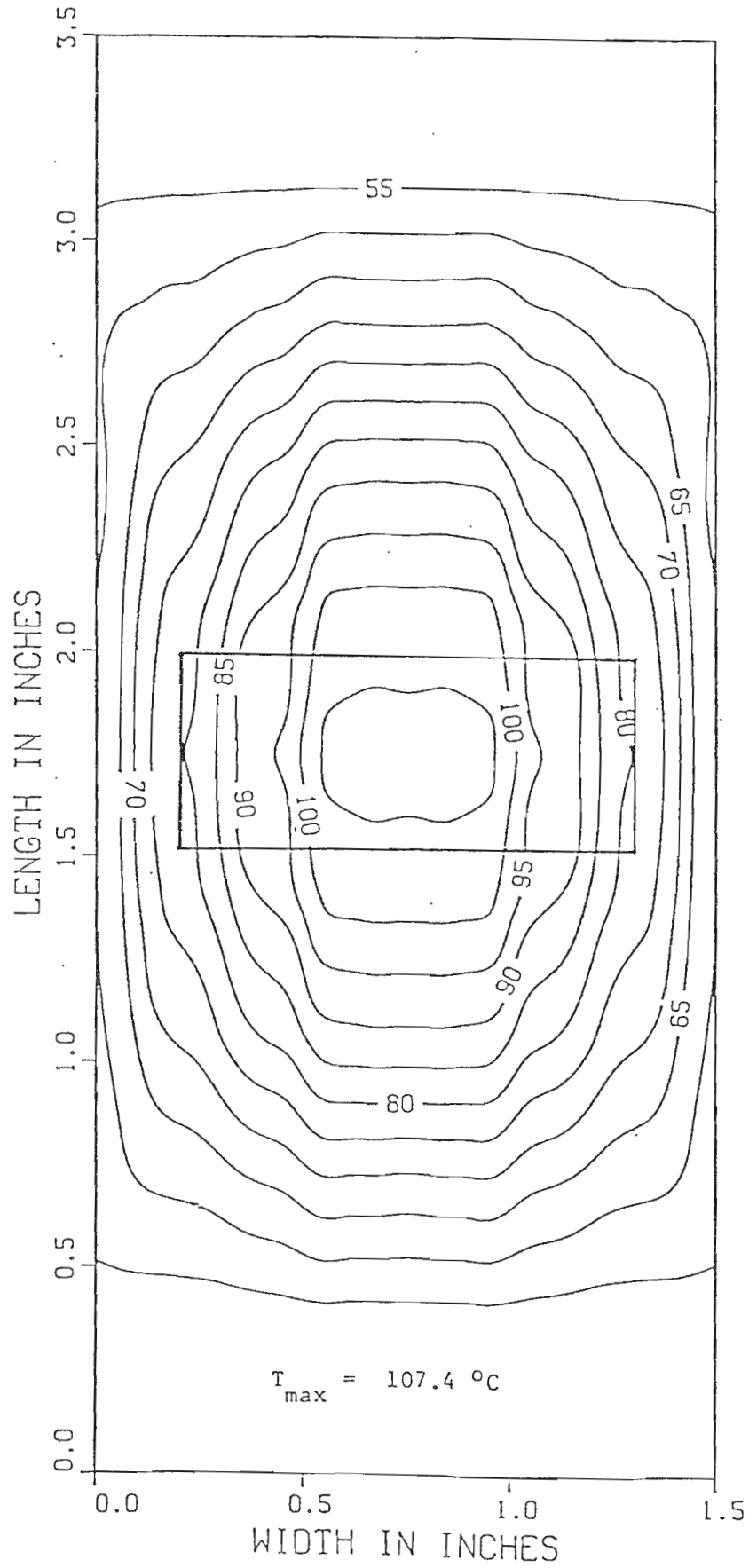


Fig. 9. Temperature distribution on the surface of the entire silicon crystal shown in Fig. 4. A Gaussian-parabolic power distribution for the incident beam is assumed. The beam footprint is also shown.

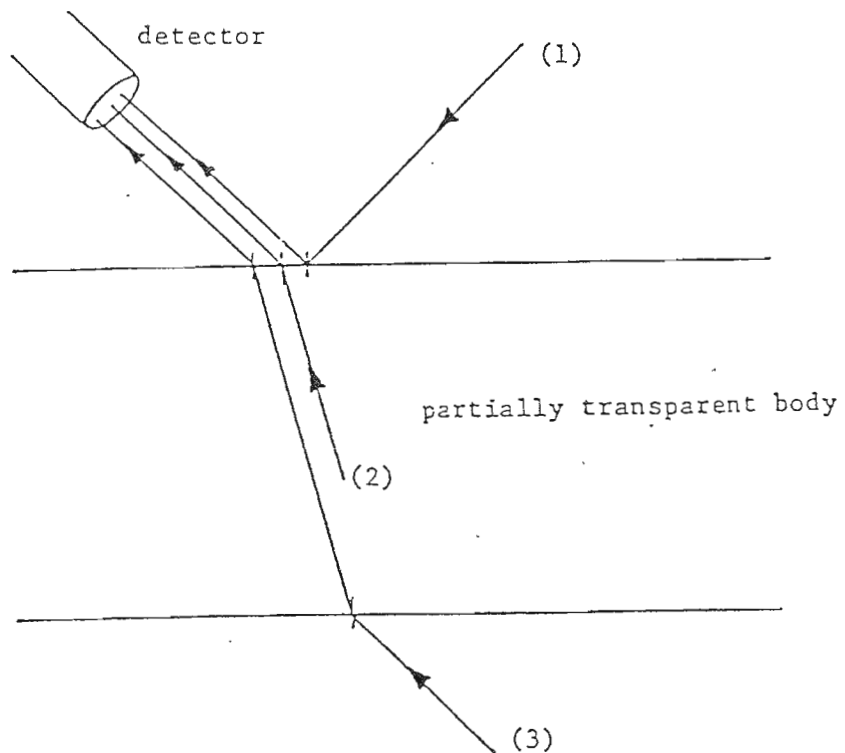


Fig. 10. Photons arriving at the detector are those (1) reflected at the top boundary, (2) emitted within the medium, and (3) emitted by the background.

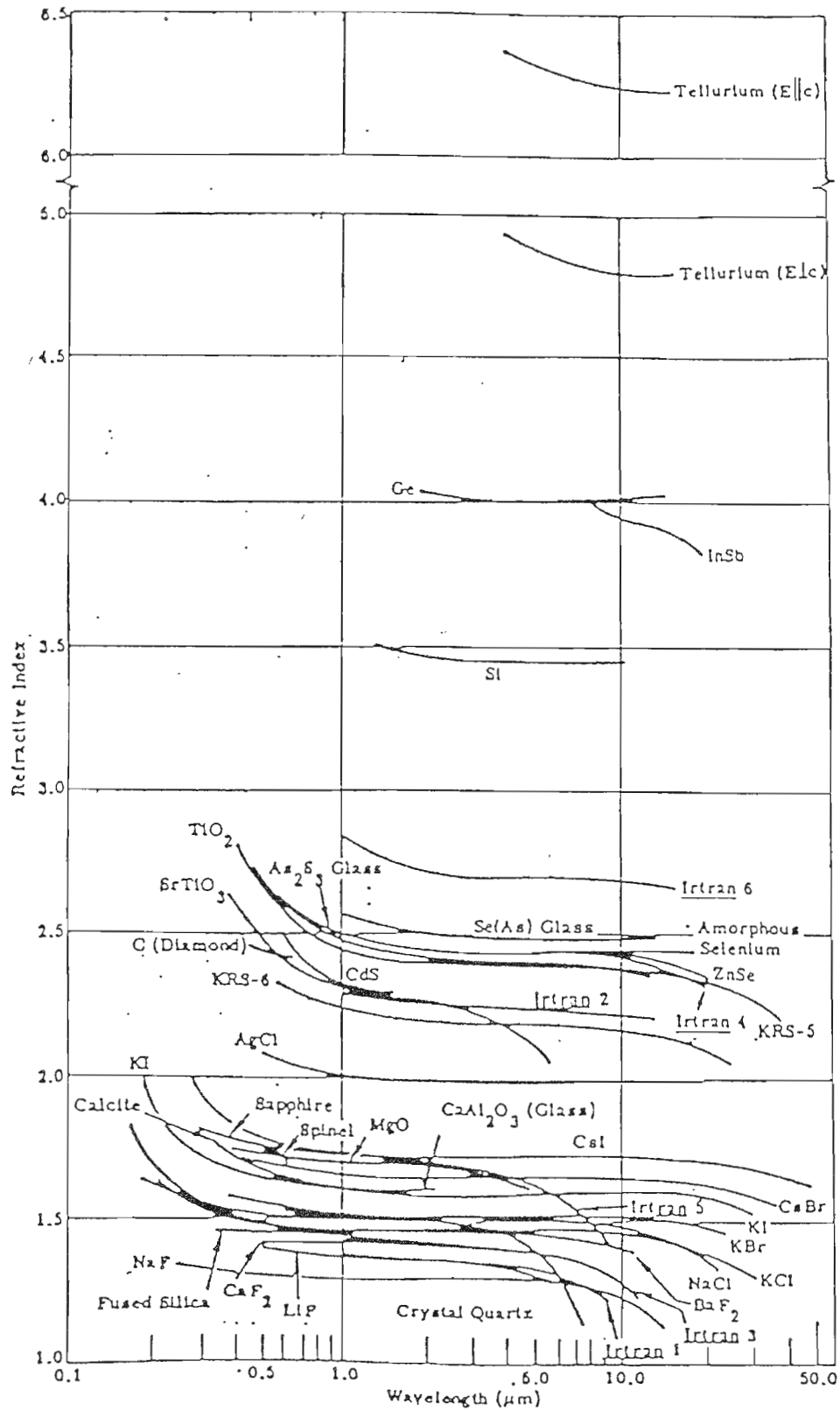


Fig. 11. Refractive index of silicon and other optical materials (borrowed from Wolfe and Zissis, 1978).

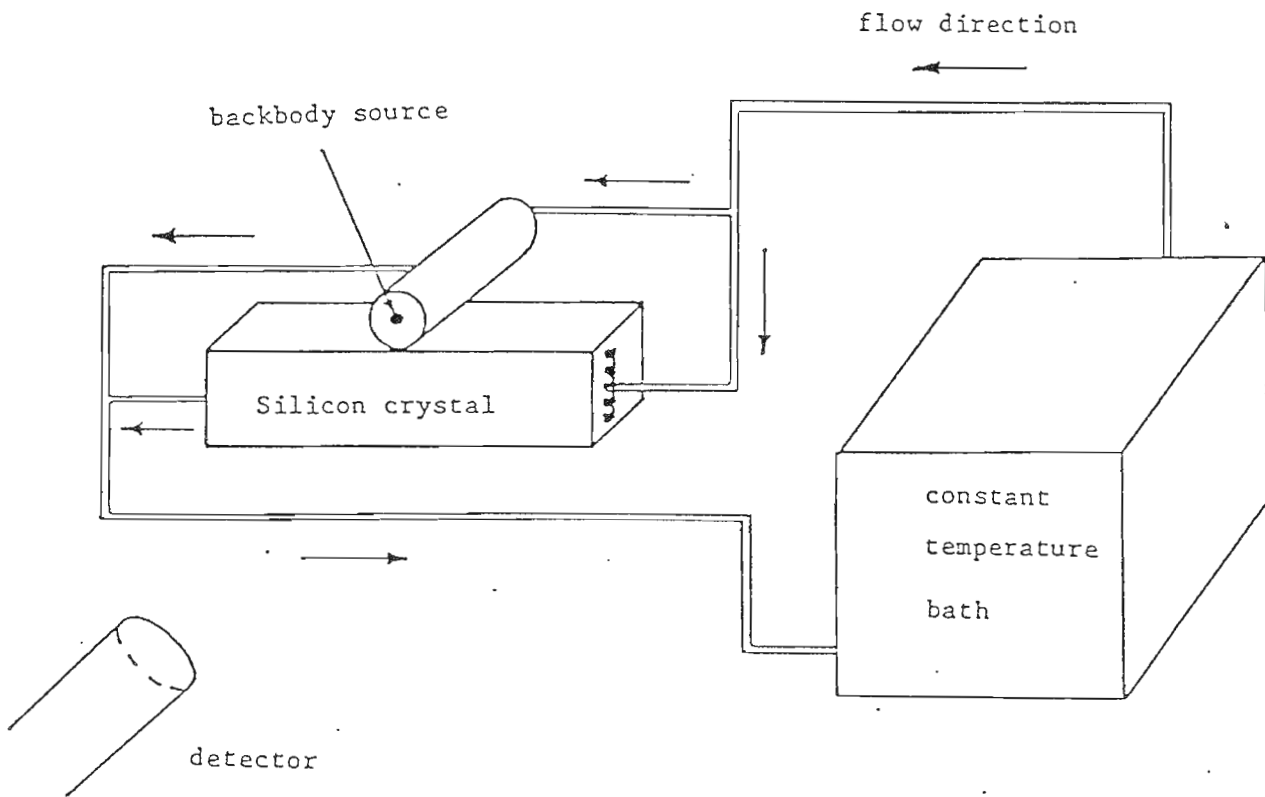


Fig. 12. The experimental setup for radiometric calibration of the INFRAMETRICS camera.

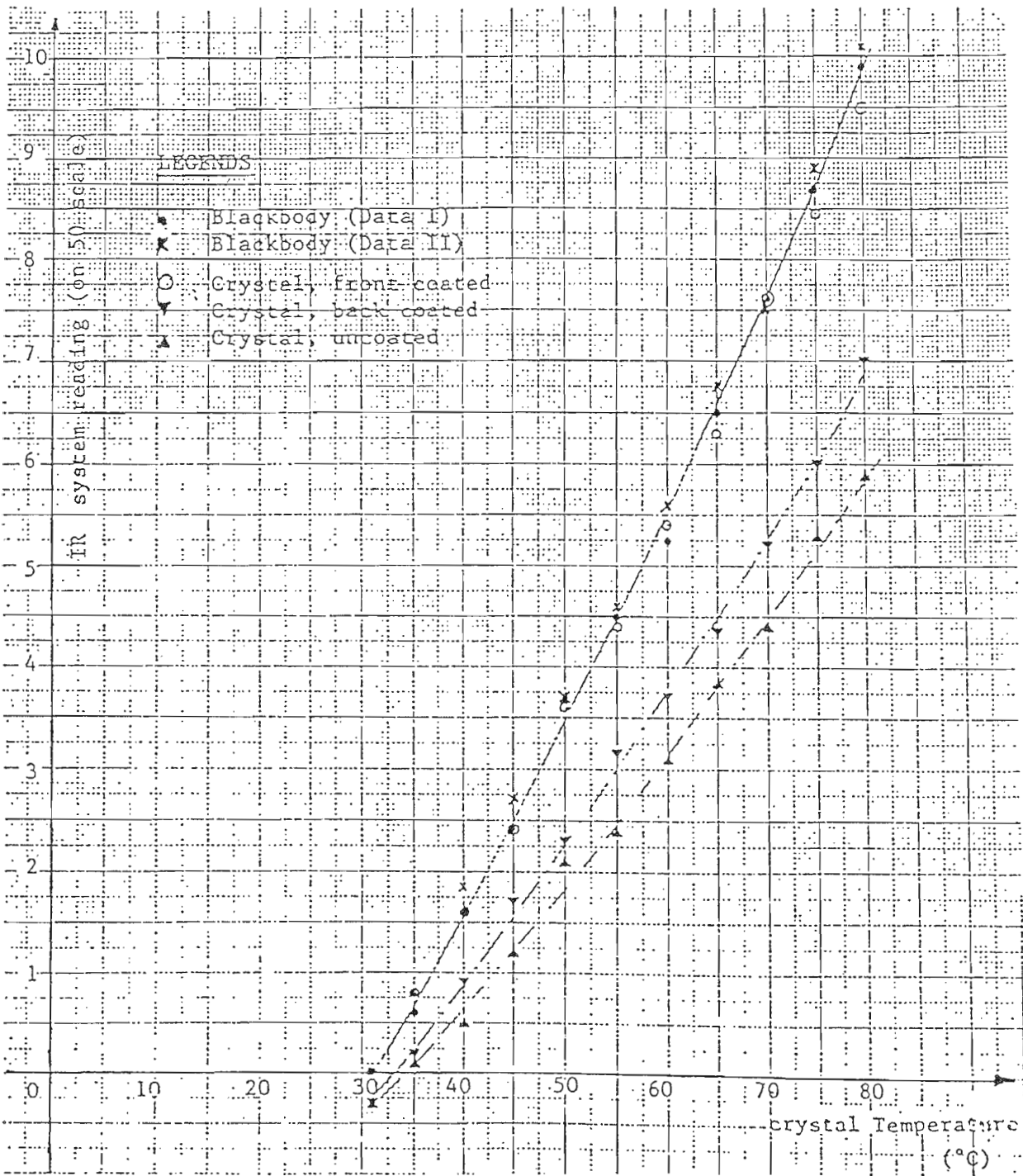


Fig. 13. Correlation curves for the 5-channel silicon crystal surface temperature.

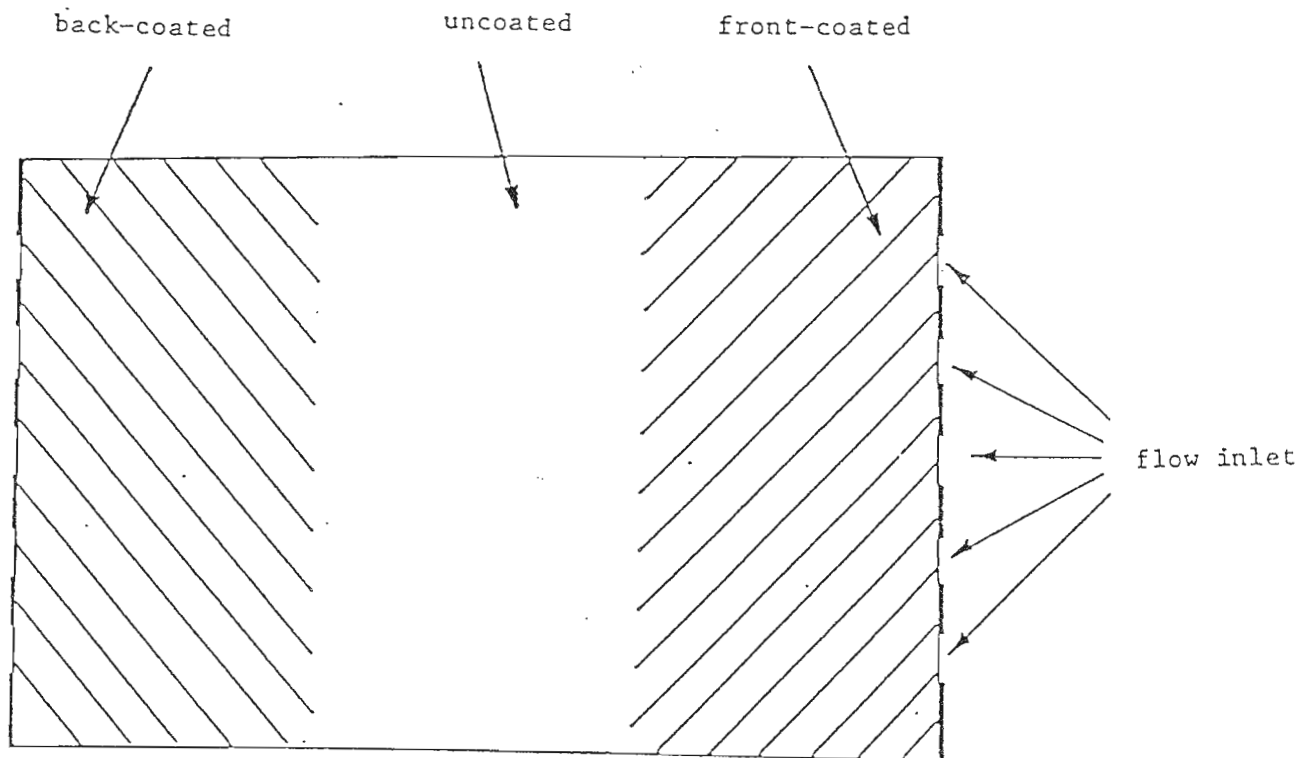


Fig. 14. Silicon crystal coatings